LTE-Advanced Network Inter Cell Interference Analysis and Mitigation using 3D Analogue Beamforming

Araz Sabir Ameen [1,2*], Djamal Berraki [1], Angela Doufexi [1], Andrew R. Nix [1*]

[1] Communication Systems & Networks Group, Department of Electrical and Electronic Engineering, University of Bristol, Bristol, United Kingdom
[2] Current Affiliation: Department of Electrical Engineering, College of Engineering, University of Sulaimani, Sulaymaniyah, Kurdistan, Iraq
[*] araz.ameen@univsul.edu.iq andy.nix@bristol.ac.uk

Abstract: This paper considers the effects of ICI on the LTE-Advanced physical layer downlink channel for different macro cell diameters and base station (BS) antenna heights with a frequency reuse factor of one and three sectors per site. A site-specific 3D ray-tracing tool is used to model the communication channel between the base stations (main and interfering links) and user equipment (UE) terminals. System performance is evaluated in terms of average spectrum efficiency, cell edge throughput, and outage probability. Two 3D analogue beamforming algorithms are proposed to mitigate the harmful effects of ICI. These are applied at the BS and/or the UE and our results are compared with a more traditional fractional frequency reuse deployment. Simulations demonstrate that our proposed beamforming algorithms provide significant system level improvements, especially for low BS antenna heights. With 10x10 and 2x2 antenna arrays at the BS and the UE respectively, the proposed MaxMin-BF algorithms can provide an average spectrum efficiency of 3.6 bps/Hz and a cell edge throughput of 0.56 bps/Hz up to a cell diameter of 1250 m. Importantly, these results satisfy the IMT-Advanced requirements for candidate 4G and beyond radio interface technologies. Furthermore, our results outperform those achieved using fractional frequency reuse.

1. Introduction

Data traffic demands in cellular networks are growing as a consequence of increasing numbers and densities of User Equipment (UE) terminals and higher data rate applications. Cost and availability of radio spectrum are limiting factors for fourth generation (4G) and beyond cellular Radio Interface Technologies (RITs). According to the requirements of the International Mobile Telecommunications-Advanced (IMT-Advanced) standard [1], candidate RITs must achieve a minimum downlink Average Spectrum Efficiency (ASE) of 2.4 bps/Hz/cell and a cell edge user throughput of 0.07 bps/Hz/cell/user respectively.

4G RITs, such as the 3rd generation partnership project (3GPP) LTE-Advanced standard, are targeting cellular deployments with a frequency reuse of one [2] and three sectors per base station (BS) site [3]. This delivers efficient utilization of the licensed spectrum with the potential for high system capacity. A significant increase in Inter Cell Interference (ICI) is expected in such deployments as a result of Inter Site Interference (ISI) and Inter Sector Interference (IsecI). This degrades the Signal to Interference plus Noise power Ratio (SINR) at the UE and has a negative impact on ASE and cell edge user throughput. According to [2], a 10 dB SINR degradation can be expected with a reuse factor of one compared with a reuse factor of three. Although the increased capacity due to greater per-cell bandwidth allocation compensates for the loss of capacity due to SINR degradation, the capacity of cell edge UEs is still adversely affected. Consequently, ICI management and mitigation is vital to ensure successful cellular deployments.

Different approaches are specified in the 3GPP LTE and LTE-Advanced standards to reduce the effects of ICI in homogenous cellular deployments. ICI Coordination (ICIC) is introduced in 3GPP Release 8 of LTE [4]. Release 11 of the 3GPP standard includes Coordinated Multi-Point (CoMP) transmission and reception [5] and Minimum Mean Square Error Interference Rejection Combining (MMSE-IRC) [6]. These techniques require estimation of the Channel State Information (CSI). The performance evaluation study in [7] showed that the efficiency of CSI feedback are challenges not currently considered in the standardisation process.

Release 12 of the 3GPP specification includes different network assisted interference cancellation techniques for the candidate LTE-Advanced UE receivers [8], which requires communication between the UE and the network. Other available UE based ICI mitigation techniques include MMSE successive interference cancellation [9] and rate splitting inter-cell codeword cancellation [10]. In these schemes, ICI is suppressed by subtracting an estimate of the interference signal from the received signal depending on information exchanged between the network and UE.

Other ICIC techniques include the algorithms proposed in [11] and [12]. In [11] the authors proposed a distributed greedy algorithm and a centralized simulated annealing algorithm to reduce the ICI in a multi cell OFDMA system. These algorithms allocate a subset of the available subcarriers to a UE in a given time slot for each cell. Both algorithms require information about the traffic and the CSI from the BSs to the UEs as well as information exchange among neighboring BSs. The authors in [12] proposed an adaptive sector coloring game (ASCG) for ICIC in a homogenous network. The ASCG technique exchanges geometric network information (GNI) instead of channel state information (CSI). Compared to the CSI based ICIC, GNI-based ICIC techniques require less computational loading and signaling overhead but at the cost of worst performance.

ICI reduction in LTE-Advanced cellular networks can be achieved by using frequency reuse factors greater than one and by employing Fractional Frequency Reuse (FFR), where the subcarriers are divided into a cell centre and a cell edge group [2]. The ICI is controlled by allocating different subcarriers and transmit power levels to the cell centre and the cell edge groups [13]. Compared to an equivalent deployment with a frequency reuse factor of one, although FFR results in increased SINR levels (especially for cell edge UEs), the ASE is typically reduced and according to [14] no significant increase is observed in cell edge UE throughput. A power management technique to reduce ICI in network MIMO is proposed in [15]. The authors showed that the proposed power management combined with a proper antenna orientation reduce the ICI and provide improved and consistent capacity performance for the UEs in the cells center and cell edge.

It is well known that cellular network performance can be increased with the use of beamforming (BF). Here linear or planar antenna arrays are used to achieve either orthogonality in the channel matrix or array gain in a specific direction. Digital BF is already included in the 3GPP technical specification for LTE-Advanced [16]. This approach is known to be more efficient in a high SINR regime since the transmitter must split its power across the different spatial streams [17]. Splitting the power at low SINR results in weakening each spatial stream which has negative impact on the achieved bit errors and overall system capacity. Furthermore, cost and complexity of digital BF increase as the number of antenna elements increase since a distinct RF chain is required for each antenna element [18] .

Analogue BF is a promising alternative technology for enhancing ASE in the low SINR regime (i.e., power and/or interference limited scenarios), especially at the cell edge. An array can be employed to increase the SINR level at the UE and allow the use of higher order modulations. Here SINR increase because of increased signal strength and/or reduced ICI [19]. BF weights of the antenna array can be selected from pre-defined codebook based on a specific criterion. For example, BF in [20] is performed at the BS and the algorithm selects a set of weights that maximizes the received signal to noise power ratio (SNR) at the UE. Similarly, the BF in [21] also aims to maximizes the received SNR at the UE but the BF is employed at both the BS and the UE. The BF algorithm selects BS and UE BF weights from a subset based on hierarchical codebooks. A maximum capacity criterion for BS and UE BF is proposed in [22] which maximizes the received SNR in the low SNR regime and improves the overall capacity for moderate and high SNR regime. Overall capacity is improved by utilizing part of received SNR to enhance the worst subcarriers in multicarrier system. In [23] an adaptive interference nulling algorithm is proposed without the need to know the direction of arrival of the interferers. The algorithm optimizes the weight of the antenna array to minimize the total output power of the beamformer while maintaining the main lobe gain.

The available ICI mitigation methods in the literature require accurate CSI at all serving BSs. They also require information exchange between different BSs and different layers of the same BS or UE protocol hierarchy. ICI mitigation is therefore sensitive to feedback overheads, delays and errors. Therefore, the objective in this paper is to analyse the effect of ICI on the performance of LTE-Advanced system with a frequency reuse factors of one, and propose two analogue BF techniques that are insensitive to feedback overhead to mitigate the effect of ICI. The aim is to satisfy the average spectrum efficiency and cell edge UE throughput requirements of the IMT-Advanced for candidate 4G RITs. The objectives of the paper can be detailed as follows:

i. To study the effect of ICI on LTE-Advanced network performance (frequency reuse factor of one) in *realistic* macro cell scenarios that follow a 3GPP three sector hexagonal grid. A map-based 3D ray tracing channel model is used to represent the propagation characteristics of the BS-UE links. The study is performed for five cell diameters (250 m, 500 m, 750 m, 1000 m, 1250 m), three BS heights (10 m, 30 m, 50 m) at a carrier frequency of 2.6 GHz in a 16-square km area in the city Centre of Bristol, United Kingdom.
ii. The effect of ICI is mitigated through analogue BF techniques that is applied to all BS-UE links in the cell centre and the cell edge using linear and planar arrays at the BS and/or UE. Our BF results are compared with a traditional FFR scheme. Two BF algorithms are proposed for use at one or both sides of the communication link. The methods rely on nulling the ICI signal and increasing the main BS signal. The study is performed assuming a (10×10) planar BS array and a (4×4, 2×2 or 1×4) UE array. This is to achieve the minimum downlink ASE of 2.4 bps/Hz/cell and the cell edge user throughput of 0.07 bps/Hz/cell/user respectively required by IMT-Advanced for the candidate 4G RITs.
   Different from the available ICI mitigation techniques in the literature, the proposed ICI mitigation techniques in this paper require no information exchange between different BSs when the BF is performed at the BS side. Furthermore, there is no need for information feedback between the UEs, the serving BS, and the interfering BSs when BF is performed at the UE side.

The remainder of the paper is organized as follows: Section 2 explains the system model including the channel model, network layout and SINR calculation, and analogue beamforming and antenna patterns. ICI results and analysis are presented in Section 3 showing the impact of the BS transmit power and height on the system performance. Section 4 introduces ICI mitigation algorithms and discusses the obtained results. Finally, conclusions are drawn in Section 5.

2. System Model

This section presents the system model of the LTE-Advanced Physical Downlink Shared Channel (PDSCH). Subsection 2.1 describes the 3D ray tracing tool used to model and generate the channel impulse response of each BS-UE link. The network layout and the SINR calculations are presented in subsection 2.2. Subsection 2.3 provides the mathematical representation used to generate the total pattern of the beamforming array. The resulted pattern is then integrated with the channel impulse response to model the communication channel between each BS-UE link. Finally, subsection 2.4 describes the RBIR simulation tool that is used to evaluate the throughput performance of each BS-UE link based on the channel impulse response and the SINR of each BS-UE link obtained from subsections 2.1, 2.2, and 2.3.

2.1. 3D Ray Tracing Channel Model

The University of Bristol's outdoor ray tracer is used in this study. The model, known as Prophecy, provides point-to-point predictions of the 3D multipath for each BS to UE link. The channel is modelled as a set of spatial and temporal MPCs with information provided on the amplitude, phase, time delay, elevation angle of arrival (AoA_{el}) and departure (AoD_{el}) and azimuth angle of arrival (AoA_{az}) and departure (AoD_{az}). The model identifies all direct, transmitted, single scattered, double scattered and multiple diffracted ray paths between the BS and UE. Physical path tracing is based on a database of irregular terrain, 3D building and foliage structures. The model was originally developed in 1995 and has enjoyed continuously development over a period of 20 years. The model's output has been validated by direct comparison with measurements at carrier frequencies ranging from 400 MHz to 2.6 GHz [24]. Fig. 1(a) shows the predicted MPCs for an example BS-UE link. Isotropic antennas are modelled at both ends of the link with specific antenna patterns applied as a post processing spatial and polarimetric convolution process.

2.2. Network layout and SINR Calculation

The LTE-Advanced system is based on a 3GPP macro cellular deployment with a frequency reuse factor of one. As shown in Fig. 1(b) each BS site consists of three sectors with a cell radius R placed on a hexagonal grid with an inter site distance of $3R$ and a cell diameter of $2R$ [3]. Within each cell, and unlike the system level simulator reported in [6], different UEs were randomly scattered at street level. The study is performed for different cell diameters and BS antenna heights at a carrier frequency of 2.6 GHz in a 4 km × 4.4 km area in the city centre of Bristol, United Kingdom. Different BS transmit powers are assumed for each of the cell diameters with parameters taken from [25]. Table 1 summarizes the system parameters used in our studies.

In Fig. 1(b) the main BS site lies at the centre with ICI caused by ISI and IsecI. The ISI is generated from different sectors of the first tier of six interfering BS sites surrounding the main BS site, while the IsecI occurs from the two other sectors within the same site as summarized in Table 2. Given the finite set of BS locations the resulting model generated an irregular hexagonal grid as illustrated in Fig. 1(c). The ray tracer was used to predict the MPCs for the main and interfering BS-UE channels. The SINR at each user location, u, associated with the main BS cell, M, and the interfering BS sites, (I: I_1, I_2, ... I_6), is given by (1):

$$SINR_{u,M} = \frac{P_{u,M}}{P_{AWGN} + \sum_{ISI} P_{u,ISI} + \sum_{I\,\mathrm{sec}\,I} P_{u,I\,\mathrm{sec}\,I}} \quad (1)$$

In (1), $P_{u,M}$, $P_{u,ISI}$, $P_{u,IsecI}$ represent the received signal strength at location u associated with the main BS sector cell, ISI cells and IsecI cells respectively. The interference power is summed across all interferers and P_{AWGN} denotes the additive white Gaussian noise, which is calculated using (2).

$$P_{AWGN} = K \times T \times B_{effec} \times F_{linear} \quad (2)$$

In (2) K represents Boltzmann's constant, T is the temperature in Kelvin, B_{effec} is the effective bandwidth (90% of the total bandwidth in an LTE-Advanced OFDM system) and F_{linear} is the noise figure (linear value). In this study, a 10 MHz LTE−Advanced bandwidth is assumed along with T=288 *Kelvin* (15°C) and F_{dB}=9 dB [3].

Table 1 Channel model parameters

Parameter		Value				
LTE Advanced Bandwidth		10 MHz				
No. of Subcarrier (N_{subc})		600				
No. of OFDM Symbols		7				
T_{slot} (ms)		0.5				
Carrier Frequency		2.6 GHz				
Environments		Bristol-United Kingdom				
Cellular Deployment		3GPP 3-sector hexagonal grid with reuse factor of one				
Minimum BS_UE distance		50 m				
Cell Diameter (m)		250	500	750	1000	1250
BS transmit power (dBm)		33	37	40	43	46
No. of UEs per sector		200	300	400	450	500
No. of BS		17				
BS antenna Height		10 m, 30 m, 50 m				
BS antenna tilt		10°				
UE sensitivity		-120 dBm				
Used Antennas		Macro-BS		Patch		UE
Antenna Beam-width	Azimuth	65º		80°		360º
	Elevation	15º		84°		36º
Array elements Spacing		$0.5\times\lambda_{2.6\ GHz}$				
Array configuration $N_{az} \times N_{el}$	BS	10 x10 planar Array				
	UE	Linear array		Planar Array		
		1x4		2x2,4x4		

Table 2 Source of ICI for different UE locations

UE location within main BS site	Source of ICI	
	IsecI	ISI
Sector1	$M_{Sector2}$, $M_{Sector3}$	$I_{1\text{-}Secor2}$, $I_{1\text{-}Sector3}$, $I_{2\text{-}Sector3}$ $I_{3\text{-}Secor1}$, $I_{3\text{-}Sector3}$, $I_{4\text{-}Sector1}$ $I_{5\text{-}Secor1}$, $I_{5\text{-}Sector2}$, $I_{6\text{-}Sector2}$
Sector2	$M_{Sector1}$, $M_{Sector3}$	
Sector3	$M_{Sector1}$, $M_{Sector2}$	

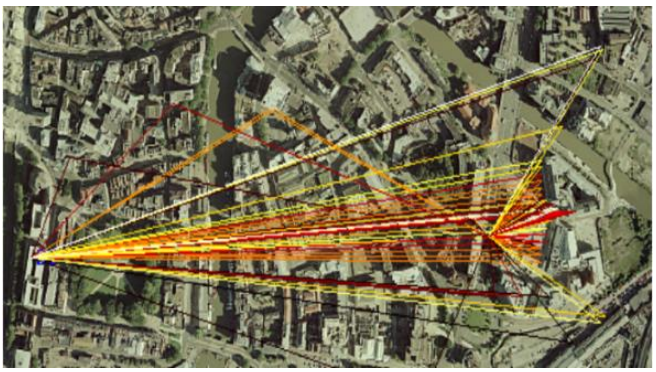

a

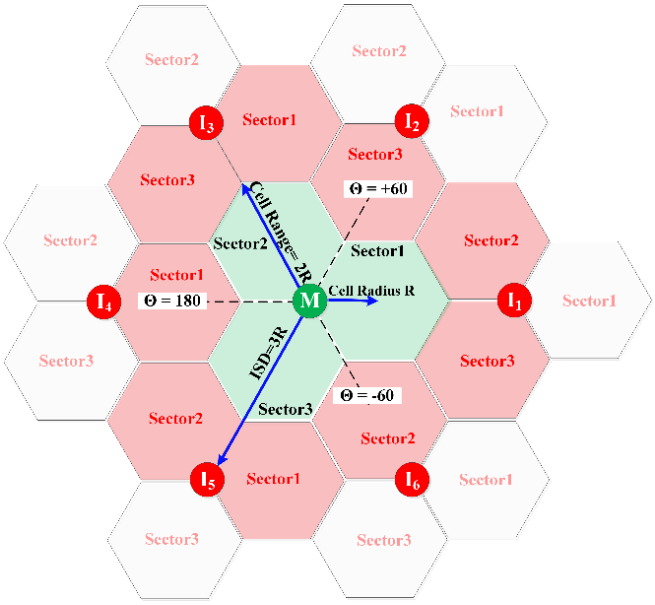

b

c

Fig. 1. *Ray tracing channel modelling and network layout*

(a) Captured MPCs for an example BS-UE link in Bristol City Centre.

(b) The 3GPP cell topology.

(c) An Example of UE distribution, main BS and interfering BS location for cell diameter of 250 m.

2.3. Analogue Beamforming and Antenna Patterns

Linear and planar antenna arrays are deployed in this study using identical antenna elements along with analogue BF to enhance the SINR in interference limited cellular networks. In comparison with a linear array, a planar array offers better pattern symmetry, lower side lobes and the ability to direct the main antenna lobe to any point in space [26]. In the planar antenna array of Fig. 2(a), (N_{az}×N_{el}) antenna elements are placed in the (y-z) plane with an inter-element spacing of d. The total pattern of the array is obtained from (3) [26].

$$y = \frac{1}{N_{az}N_{el}} \sum_{m=1}^{Naz} \sum_{n=1}^{Nel} E_{m,n} \cdot W_{m,n} \tag{3}$$

In (3), $E_{m,n}$ can be calculated using (4) based on the reference phase pattern E and represents the pattern of antenna element m,n placed at location [$dx_{m,n}$, $dy_{m,n}$, $dz_{m,n}$]. Note that the direction of observation in this case is defined by the elevation angle θ and the azimuth angle ϕ as shown in the coordinate system of Fig. 2(a). Similarly, the main beam can be directed to a specific direction defined by the elevation angle θ_0 and the azimuth angle ϕ_0 through adjusting the weight $W_{m,n}$ of element m, n using (5).

$$E_{m,n} = E.e^{j\frac{2\pi}{\lambda}(dx_{m,n}\sin\theta\cos\phi + dy_{m,n}\sin\theta\sin\phi + dz_{m,n}\cos\theta)} \tag{4}$$

$$W_{m,n} = e^{-j\frac{2\pi}{\lambda}(dx_{m,n}\sin\theta_0\cos\phi_0 + dy_{m,n}\sin\theta_0\sin\phi_0 + dz_{m,n}\cos\theta_0)} \tag{5}$$

$$dx_{m,n} = 0 \tag{6}$$

$$dy_{m,n} = (m-1)\times d \tag{7}$$

$$dz_{m,n} = (n-1)\times d \tag{8}$$

The antenna patterns used in this study were obtained from anechoic chamber measurements performed at the University of Bristol [27]. All patterns we captured in 3D and include phase, polarization and directivity information. Since polarization is considered in the study, the reference phase pattern E in (4) is substituted by the elevation and azimuth polarization patterns E_θ and E_ϕ respectively. The array patterns obtained from (3) are convolved spatially with the spatial and temporal multipath components obtained from the 3D ray tracer for each BS-UE link. Different types and numbers of array elements are used at each side of the communication link as follows:

i. NoBF: BF is not applied at either side of the link. The Macro BS and UE radiation patterns shown in Fig. 2(b) and Fig. 2(c) respectively are used for the links.
ii. BS side BF: Fig. 2(d) shows the measured pattern of a single element in the BS array. An array formed from (10×10) patch elements is deployed in the (y-z) plane. The UE pattern of Fig. *2*(c) is used in this configuration.
iii. UE side BF: In this case BF is applied only at the UE. The BS uses the pattern shown in Fig. 2(b).
iv. Combined BF: BF is performed at both ends of the link. The array patterns described in cases (ii) and (iii) above are applied to the BS and UE respectively.

Fig. 3(a) shows an example pattern obtained from 100 patch antenna elements arranged as 10x10 grid at the BS.

Here the antenna weights, $\boldsymbol{W_{m,n}}$, $\{\boldsymbol{m}: \boldsymbol{0\ to\ 9},\ \boldsymbol{n}: \boldsymbol{0\ to\ 9}\}$, are calculated using (5) with θ_0 and ϕ_0 replaced by 30° and 45° respectively. The antenna pattern at location (m, n) is calculated using (4) then the total pattern of the array is calculated using (3). Fig. 3(b) shows the total power pattern from the 2×2 rectangular array of UE elements.

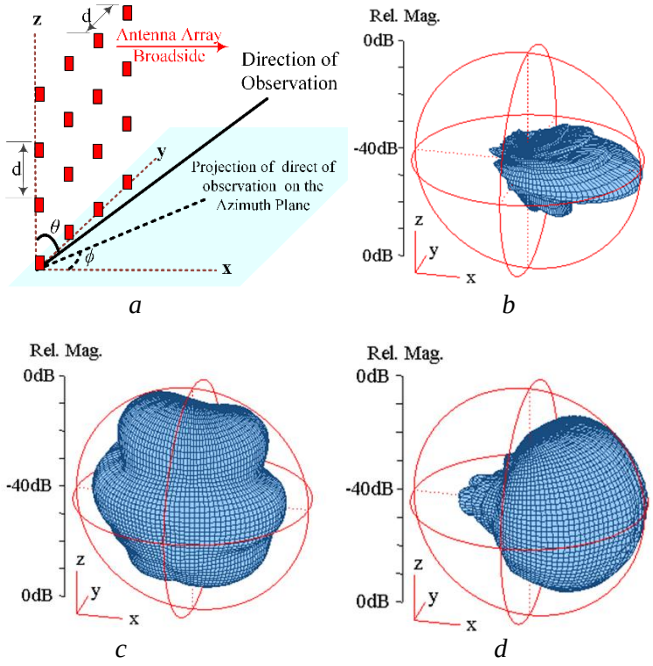

Fig. 2. *Antenna co-ordinate system and total power radiation patterns*

(a) 3D Co-ordinate System.
(b) Macro BS antenna total power radiation pattern
(c) UE antenna total power radiation pattern
(d) Patch antenna total power radiation pattern

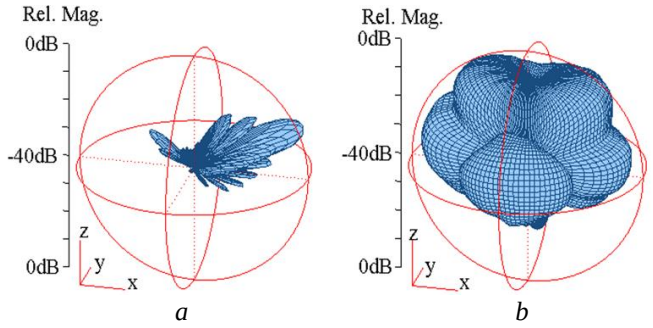

Fig. 3. *Example total power radiation patterns of antenna array.*

(a) 10x10 array of Patch elements.
(b) 2x2 array of UE antenna elements.

2.4. RBIR Link Level Abstraction

The performance of the LTE-Advanced PDSCH is evaluated for five cell diameters and three BS antenna heights. Performing bit accurate physical layer simulations to estimate statistically relevant system level performance for large numbers of BS-UE links and for many different Modulation and Coding Schemes (MCS) is time consuming. Instead, the Received Bit mutual Information Rate (RBIR) abstraction technique [28] can be used as a computationally efficient alternative to bit level simulation. In [29] we reported excellent agreement between bit level simulation and RBIR abstraction, with the latter running around 300 times faster on the same computing platform.

The combined channel and antenna impulse response for each serving BS-UE link is converted into the frequency domain and used as the input into our PDSCH RBIR abstraction engine to estimate the instantaneous packet error rate (PER) for 10 MCS modes at the average SINR determined by (1). A link adaptation algorithm is applied to select the MCS mode that maximizes the data throughput (*THR*) of each link. The LTE-Advanced PDSCH throughput is calculated using (9) [30] assuming perfect channel knowledge at the receiver. No reference signals are used to estimate the communication channel at the receiver.

$$THR_{MCS} = R_{MCS} \times (1 - PER_{MCS}) \tag{9}$$

In (9) R_{MCS} represents the peak error free data rate for the considered MCS mode which can be calculated using (10), and PER_{MCS} is the achieved PER for the considered MCS determined using the PDSCH RBIR abstraction engine. R_{MCS} is a function of modulation order (k_m), the coding rate (R_c), the number of active subcarriers (N_{subc}) and the number of OFDM symbols (N_{symb}) in the time slot (T_{slot}). Table 1 summarizes the system parameters used here while **Table** 3 lists the value of R_{MCS} for each considered MCS mode.

$$R_{MCS} = \frac{k_m \cdot R_c \cdot N_{subc} \cdot N_{symb}}{T_{slot}} \tag{10}$$

Table 3 List of MCS Modes and Peak Error Free Data Rates

MCS	Modulation	Code rate	R_{MCS} (Mbps) for SISO
1	QPSK [k_m=2]	1/3	5.6
2		1/2	8.4
3		2/3	11.2
4		4/5	13..44
5	16QAM [k_m=4]	1/2	16.8
6		2/3	22.4
7		4/5	26.88
8	64QAM [k_m=6]	2/3	33.6
9		3/4	37.8
10		4/5	40.32

3. ICI Results and Analysis

This section presents the LTE-Advanced PDSCH simulation results for a single stream for theoretic deployments in Bristol at a carrier frequency of 2.6 GHz. The results are presented using metrics such as SNR, SINR, path loss, Line of Sight (LoS) probability, ASE, cell edge throughput, and UE outage probability. Subsection 3.1 shows the impact of BS transmit power on the ASE. The impact of the BS antenna height on the SINR and SNR is analysed in subsection 3.2, while subsection 3.3 presents the impact of the BS antenna height on the ASE, cell edge UE throughput, and the user outage probability. These parameters are defined in [1] as follows:

- Average Spectrum Efficiency is measured in bit/second/Hz/Cell (bps/Hz/Cell) and defined as the aggregate throughput for all users normalised by the overall cell bandwidth and the number of cells.

- Cell edge UE throughput represents the 5% point on the cumulative distribution function (CDF) of the UE throughput normalised by the total cell bandwidth.
- User outage probability: A UE is considered to be in outage if its throughput drops to zero.

Note that the path loss is calculated per UE from the ray tracing predictions and the mean path loss models shown in this section are included to support our conclusions.

3.1. Impact of BS Transmit Power on ASE

This section studies the effect of the BS transmit power on ASE to justify the selected values of the BS transmit power for different cell diameters in Table 1. The study is performed for BS transmit power range from 20 dBm to 50 dBm considering ICI. The ASE versus BS total transmit power for different BS antenna heights and a cell diameter of 750 m is shown in Fig. 4(a) while Fig. 4(b) considers different cell radiuses for a BS antenna height of 30 m. Both figures show that the selected BS total transmit power (Pt) in the study provide at least 90% of the achievable ASE when the total transmit power set to 50 dBm. This confirms the proper selection of the BS transmit power for different cell diameters based on [25] . Any increase in the total transmit power beyond the selected values in Table I have no significant impact on the system performance.

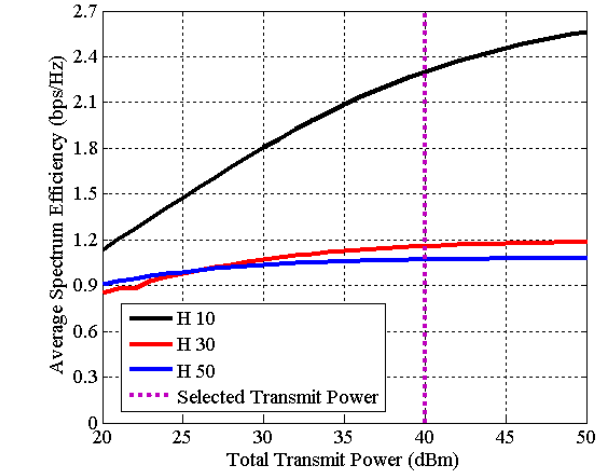

a

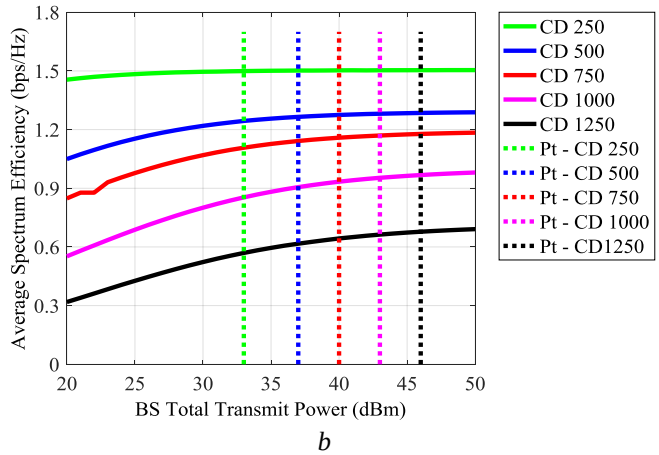

b

Fig. 4. *ASE versus BS Transmit Power for different BS antenna heights and cell diameters (CD).*

(a) Different BS antenna heights, cell diameter =750 m
(b) Different cell diameters with BS antenna height of 30 m

3.2. Impact of BS Antenna Height on SINR and SNR

The effect of BS antenna height on the SNR and SINR statistics is shown in Fig. 5(a) for a cell diameter of 750 m. As expected, the SNR level increases with increasing BS antenna height. This is the result of lower path loss to the UEs as the BS height increases (see Fig. 5(b)). A major contributor to the lower path loss is the increased LoS probability for the main BS-UE links (rising from 3.6% and 5.4% for BS heights of 10 m and 30 m respectively to 12.2% for a height of 50 m (see Table 4).

In contrast to the above, the SINR graphs presented in Fig. 5(a) show a very different trend. The inter site interfering BSs with the highest antenna heights experience the lowest path loss values (shown as dashed lines in Fig. 5(b)). This has a negative impact on the SINR level. As reported in Table 4, increased ISI with increased interfering BS antenna height is also a result of increased LoS probabilities. For BS antenna heights of 30 m and 50 m the path loss to the ISI BSs is slightly more than the corresponding main BS. This is not the case with a BS antenna height of 10 m, where the interfering BS-UE path loss is significantly higher than the main BS-UE path loss.

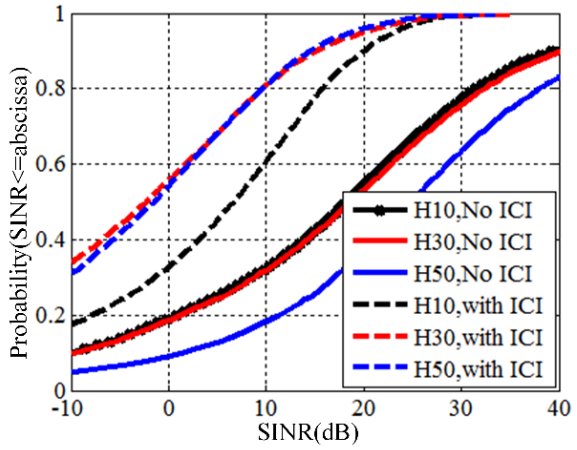

a

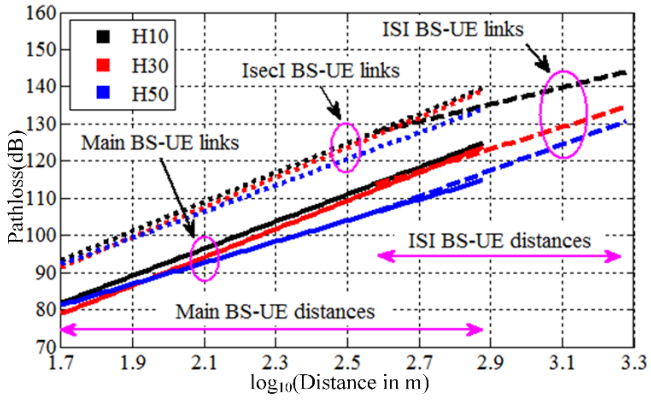

b

Fig. 5. *SNR, SINR and mean path loss model for 3GPP deployment (different BS antenna heights, cell diameter of 750 m)*

(a) SINR and SNR
(b) Best Fit Pathloss Model

For a main BS-UE link, each of its interfering links is considered to be in outage if the power sum of all interfering MPCs is less than the UE sensitivity (assumed to be 120 dBm in this study). As reported in Table 4, the outage probability for 10 m BSs is 65.2%. This drops to 27.6% and 13.4% for interfering BS heights of 30 m and 50 m respectively. Fig. 5(b) also shows slight differences in the path loss of IsecI BS-UE links for different BS heights. Overall, as confirmed by Fig. 5(a), the SINR statistics are better for 10 m BS heights and degrade with increasing BS height.

Table 4 List of LoS and ISI Link Outage Probabilities for Cell Diameter of 750 metres

Parameter	BS Antenna Height (m)		
	10	30	50
LoS Probability of Main BS-UE links	3.6 %	5.4 %	12.2 %
LoS Probability of ISI BS-UE links	0.9 %	1.4 %	3.4 %
ISI BS-UE links Outage Probability	65.2 %	27.6%	13.4%

3.3. Impact of BS Antenna Height on ASE, Cell Edge Throughput and Outage Probability

The ASE is compared for different cell diameters and BS antenna heights in Fig. 6(a). It is clear from the figure that when ICI is considered a 10 m BS height offers the best ASE for all cell diameters with a maximum ASE value of 2 bps/Hz/cell. In contrast, the ASE graphs without the effect of ICI clearly shows better performance for higher BS antenna heights. Considering the 10 m BS antenna height, Fig. 6(a) also shows that ASE decreases as the cell diameter increases. In addition, Fig. 6(b) shows the CDFs of the UE normalized throughput for different cell diameters. The 5% UE throughput corresponds to zero for all cases, which means that the cell edge throughput is equal to zero.

The achieved values of the ASE and cell edge throughput considering ICI are less than the IMT-Advanced requirement of 2.4 bps/Hz/cell and 0.07 bps/Hz/cell/user respectively. Therefore, SINR enhancement is *vital* to improve the ASE and cell edge throughput. For this purpose, two different analogue BF techniques are proposed in Section 4. These are then compared against the FFR technique.

Table 5 lists the cell edge throughputs and outage probabilities for different cell diameters and BS antenna heights for two different cases; with and without the effects of ICI. In both cases the outage probability increases with increasing cell diameter with the lowest value observed for a cell diameter of 250 m. Unlike the ICI case, higher cell edge throughputs and lower outage probabilities are observed for 50 m BS antenna heights compared to the 10 m antenna height when neglecting ICI.

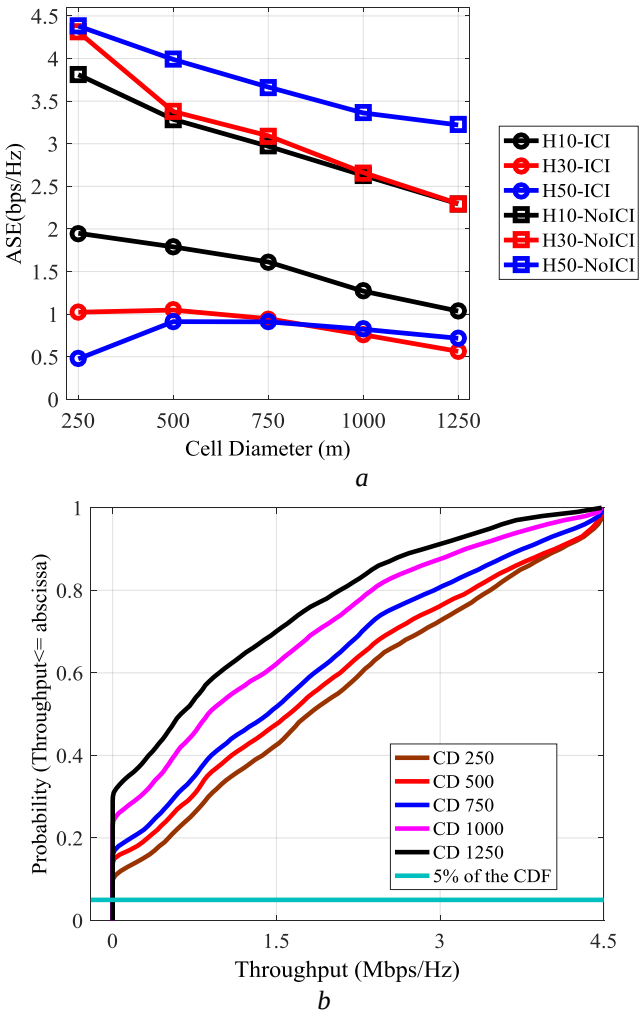

Fig. 6. *Average spectrum efficiency and CDF of UE throughput*

(a) Average spectrum efficiency for different BS antenna heights and cell diameters with and without ICI.

(b) CDF of UE throughput for different cell diameters (CD) for 10 m BS antenna height with ICI.

Table 5 List of Cell Edge Throughput and Outage Probability

	Cell Diameter (m)	Cell Edge UE Throughput (Mbps/Hz)			UEs Outage Probability		
		H10	H30	H50	H10	H30	H50
With ICI	250	0	0	0	0.11	0.20	0.20
	500	0	0	0	0.14	0.30	0.30
	750	0	0	0	0.15	0.35	0.33
	1000	0	0	0	0.22	0.44	0.40
	1250	0	0	0	0.27	0.53	0.44
Without ICI	250	0.68	3.41	3.96	0.02	0.00	0.00
	500	0.00	0.00	1.38	0.06	0.06	0.01
	750	0.00	0.00	0.17	0.08	0.08	0.04
	1000	0.00	0.00	0.00	0.13	0.13	0.07
	1250	0.00	0.00	0.00	0.17	0.17	0.08

4. ICI Mitigation

Next, we investigate the use of analogue beamforming to reduce the effects of ICI in an LTE-Advanced cellular network. The antenna array is defined by $N_{az} \times N_{el}$ elements arranged uniformly in the elevation plane. BF is performed at the BS using a 10×10 array and at the UE side using 1×4, 2×2, or 4×4 arrays. The study is performed assuming the interfering BSs do not exchange information with the serving BS. Furthermore, when considering BF at the main BS we assume random BF at the interfering BS sites.

As explained in Section 2.3, BF is performed in the main cell by applying weights to the antenna elements. These weights are calculated using (5) as a function of the antenna element position and the desired steering direction described by θ_0 and ϕ_0 in the elevation and azimuth planes respectively. Three different algorithms are used to calculate the array weights for SINR enhancement. The algorithms either 1) increase the received signal strength, 2) null the ICI or 3) perform a mixture of the two as described in subsections 4.1, 4.2, and 4.3 respectively. The performance of the three BF algorithms is also compared with the FFR technique discussed in subsection 4.4. Finally, subsection 4.5 shows the impact of the array configuration on the system performance and the relation between the throughput and other channel parameters.

4.1. Maximum Ray Power BF (MaxRP-BF)

In this algorithm, the values of θ_0 and ϕ_0 in (5) are substituted by the departure or arrival angles of the maximum power MPC at the BS or UE respectively as summarized in Algorithm 1. As mentioned in Section 2.1, the angular information of the maximum power MPC of each BS-UE link is obtained from the ray tracer tool, however practically this can be estimated using special techniques. The effectiveness of this approach in terms of increasing the serving BS signal strength is investigated at both the BS and UE. Fig. 7(a) shows the ASE for the different BF algorithms and for a number of cell diameters. Results without BF and ICI are also included in the figure for comparison. As mentioned in Section 3, better performance is observed for BS antenna heights of 10 m when ICI is included in the simulation. In the ICI free case a 50 m BS height yielded the best performance. Hence, the results in this section assume a BS height of 10 m in all cases other than the interference free scenario, where a 50 m BS height is applied.

Algorithm 1: Procedure of MaxRP-BF	
1	Find the maximum power MPC

2	if BS side BF:
	θ_0 = elevation departure angle of the maximum power MPC
	ϕ_0 = azimuth departure angle of the maximum power MPC
	else if UE side BF:
	θ_0 = elevation arrival angle of the maximum power MPC
	ϕ_0 = azimuth arrival angles of the maximum power MPC

3	Calculate weight $W_{m,n}$ using (10) for each antenna element

Comparing the ASE graphs of Fig. 7(a), MaxRP-BF at the BS exceeds the IMT-Advanced requirement of 2.4 bps/Hz. Furthermore, the performance of MaxRP-BF at the UE is close to the NoBF case and lower than the IMT-Advanced requirement for all cell diameters. MaxRP-BF is more effective at the BS for two reasons. Firstly, considering the power CDF graphs in Fig. 7(b), MaxRP-BF at the BS results in higher total received power than MaxRP-BF at the UE. This is a result of the higher directivity gain obtained from the 10×10 array at the BS (see Fig. 3(a)) compared to the 4×4 array at the UE. Secondly, MaxRP-BF at the UE leads to ICI enhancement in addition to the main signal power, while the application of random BF at the interfering BSs reduces the ICI power at the UE.

4.2. Proposed Minimum ICI BF (MinICI-BF)

This section proposes a novel algorithm for selecting the BF weights for analogue BF. The available techniques in the literature enhance the system performance by increasing the received signal strength at the UE [20]- [22]. In contrast our proposed MinICI-BF algorithm aims to minimize the total received ICI power by applying a predefined set of weights that provide the highest SINR value (see algorithm 2). This algorithm is proposed for exclusive use at the UE, where information exchange with any BS (including the main BS) is not required. Different weights are calculated by applying different values of θ_0 and ϕ_0 in increments of Δx, where Δx is assumed to be 30° for a planar array and 10° for a linear array.

The ASE results for MinICI-BF and for different array configurations are presented in Fig. 7(a). The results show a performance increase compared to the cases of UE MaxRP-BF and NoBF. For MinICI, the performance of 4×4 is greater than the 2×2 and 1×4 arrays. The 2×2 and 1×4 arrays fail to achieve the ASE requirements of 2.4 bps/Hz for cell diameters of 500 m and above. The 4x4 array can provide an ASE of 2.4 bps/Hz for cell diameters up to 750 m. Focusing on the performance difference between planar and linear array elements (keeping the total number of elements constant), our CDF plots of the received main and ICI power in Fig. 7(c). show that the planar array performs slightly better than the linear array. The CDF data shows a slightly lower level of received ICI power when the planar array is used.

It can be seen from Fig. 7(c) that the ability of the MinICI-BF algorithm to reduce ICI is better than its ability to increase the main signal strength. This explains why the 1×4 and 2×2 MinICI-BF outperforms the 4×4 MaxRP-BF at the UEs despite the higher array gain with more antenna elements. This explains the ability of our proposed MinICI-BF algorithm to increase system performance. However, the performance is worse than the interference-free scenario.

To see the impact of the different BF algorithms on the cell edge users, Table 6 list the cell edge throughput for each algorithm for the same scenarios as those depicted in Fig. 7(a). As mentioned in the introduction, the IMT-Advanced target for cell edge throughput is 0.07 bps/Hz. It is clear from Table 6 that among the aforementioned algorithms the cell edge throughput target is only satisfied with *i*) the 10×10 BS array with the MaxRP-BF algorithm for cell diameters up to 1000 m and *ii*) the 4×4 UE array with the MinICI-BF algorithm for a cell diameter of 250 m. In the following section our proposed MinICI-BF approach, which is applied

exclusively at the UE side, is extended by also adding MaxRP-BF at the BS.

4.3. Combined MaxRP and MinICI BF

Given the effectiveness of the MaxRP-BF and MinICI-BF algorithms to enhance SINR when applied at the BS and UE respectively, further system performance can be achieved by running both algorithms concurrently in a new algorithm (MaxMin-BF). The BS performs MaxRP-BF to increase received main received power at the UE while the UE minimizes the ICI power through MinICI-BF as summarized in Algorithm 3.

In Fig. 7(a) the MaxMin-BF results are presented for a 10×10 BS antenna array and 2×2 and 1×4 UE arrays. The ASE in both cases outperforms the interference-free results for a cell diameter of 750 m and above. Very close results are also observed for a cell diameter of 500 m. Fig. 7(d) shows that the SINR level of the MaxMin-BF algorithm exceeds the interference-free scenario. Moreover, from Table 6 it can be seen that the IMT-Advanced cell edge throughput requirement is satisfied for all cell diameters when 2×2 and 1x4 UE arrays are deployed.

Algorithm 2: Procedure of MinICI-BF	
1	Determine a codebook of antenna weights: For θ_0 =0° to 180° in steps of Δx For ϕ_0 =0° to 360° in steps of Δx Calculate BF weights $W_{m,n}$ using (10) for each antenna element (m,n)
2	For each set of BF weights in the codebook: Calculate received SINR at the UE Choose the BF weight that results in the lowest received interfering power and maximize the received SINR.

Algorithm 3: Procedure of MaxMin-BF	
1	Apply MaxRP-BF (Algorithm 1) at the BS side.
2	Apply MinICI-BF (Algorithm 2) at the UE side.

Table 6 List of Cell Edge Throughputs for Different BF Algorithms

Case	Cell Edge throughput (bps/Hz)				
	Cell Diameter (m)				
	250	500	750	1000	1250
No-BF, With ICI	0	0	0	0	0
MaxRP-BS10×10	0.748	0.418	0.392	0.090	0
MaxRP-UE4×4	0	0	0	0	0
MinICI-UE4×4	0.297	0	0.004	0	0
MinICI-UE2×2	0.000	0	0	0	0
MinICI-UE1×4	0	0	0	0	0
MaxMin, BS10×10, UE2×2	1.982	1.090	1.078	0.643	0.562
MaxMin, BS10×10, UE1×4	1.698	0.913	0.888	0.492	0.336
No-BF, No ICI	1.210	0.512	0.534	0.002	0
FFR	0.04	0	0	0	0

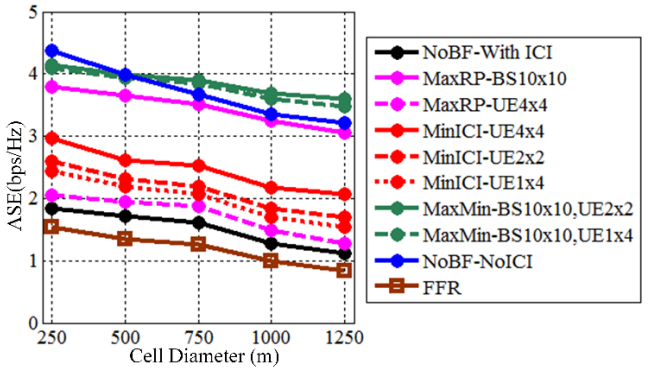

a

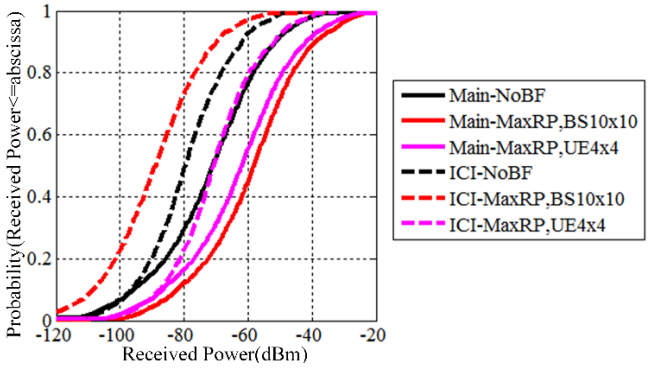

b

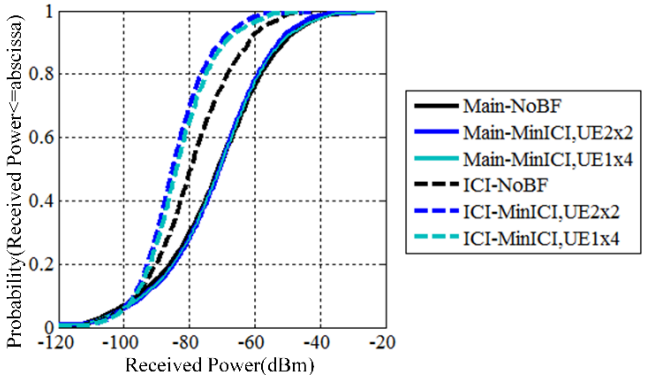

c

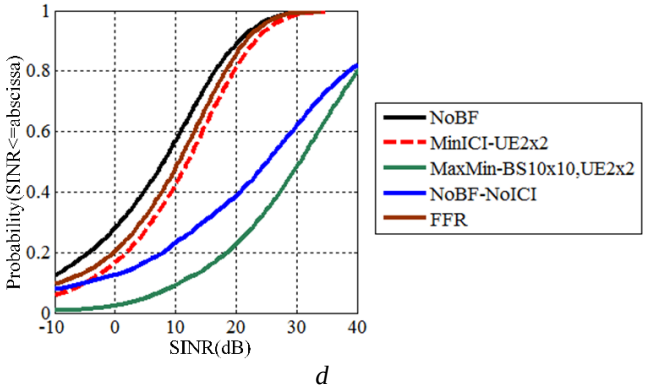

d

Fig. 7. *Performance of different BF algorithms a BS antenna height of 10 m.*
(a) Average Spectrum Efficiency for different cell diameters
(b) CDF of the received main and ICI powers of MaxRP-BF and No-BF for a cell diameter of 500 m.
(c) CDF of the received main and ICI powers of MinICI-BF and No-BF for a cell diameter of 500 m.
(d) CDF of the SINR for different simulation scenarios for a cell diameter of 750 m.

4.4. Comparison with Three Sector FFR Approach

In this section the performance of the proposed BF algorithms is compared against the three-sector FFR deployment described in [31]. Each sector is divided into cell centre and cell edge groups. In this study 50% of the available radio resources are assigned to the cell centre group with the remaining divided equally between the three cell edge group sectors. Furthermore, the centre range is assumed to extend to 60% of the cell edge range. The selection of these FFR parameters is based on recommendations in [31] for optimal performance.

It is clear from Fig. 7(a) that the ASE for the FFR scenario is lower when compared with the other scenarios, including the NoBF case, due to the use of spectrum partitioning. The outage probability results in Fig. 8 show significantly better performance for the FFR technique compared with MaxRP-BF performed at the UE and the NoBF case for all cell diameters. FFR outage performance is also slightly better than the MinICI with 1×4 arrays performed at the UE for a cell diameter of 250 m. However, all other BF algorithms outperform the FFR scenario. The cell edge throughput results in Table 6 show that the use of FFR is unable to satisfy the cell edge throughput requirement of IMT-Advanced for all cell diameters. This confirms the conclusion of [14]. Finally, we compare the SINR graphs of Fig. 7(d) to the FFR scenario with the MinICI-BF algorithm using a 2×2 UE array. By combining a 2×2 UE array with the MinICI-BF algorithm it is possible to exceed the SINR levels using FFR.

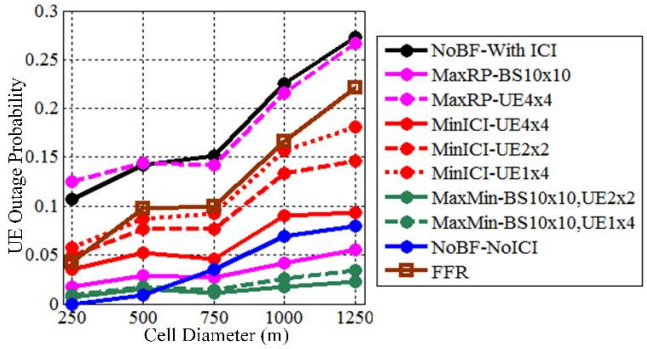

Fig. 8. *Outage probability for different BF algorithms and cell diameters for BS antenna height of 10 m.*

4.5. Impact of the Array Configuration on the Performance

This section investigates the impact of the number of antenna elements in the BF array and their arrangement as linear or planar array on the UE throughput, the SINR level at the UE, the K factor, and the Root Mean Square (RMS) Delay Spread (DS). We also determine a relation between the throughput at the UE and the other aforementioned channel parameters. For this analysis we consider the different array configurations of the proposed MinICI algorithm that is applied at the UE using 4x4, 2x2, and 1x4 array configurations. The throughput and the channel parameters for the No-BF case are also included in the analysis for comparison and reference.

As mentioned previously, the proposed MinICI-BF algorithm aims to minimize the total received ICI power by applying a predefined set of weights that provide the highest SINR value. Fig. 9(a) shows the CDF graphs of SINR level at the UEs for the different array configurations of the MinICI algorithm. It is clear from the figure that the MinICI algorithm in enhancing the SINR as the number of antenna elements in the array increases. The SINR enhancement is due to reduction in the received ICI power combined with the increase in the total received power from the serving BS. The BF algorithm increases the received power from the serving BS in a specific direction while reducing the received power from other directions. This results in a received multipath component (MPCs) with a high power dominant MPC compared to the other MPCs. This in turn leads to increase in the K factor and decrease in the RMS DS with the increase in the number of elements in the array as shown in the CDF graphs of the K factor and the RMS DS in Fig. 9(b) and Fig. 9(c) respectively.

Fig. 9(d) show that the throughput at the UE increases as number of the elements in the array increases. This increase in the throughput is contributed to the increase of the SINR levels, increase in the K factor, and the decrease in the RMS DS at the UE as the number of elements in the array increases from one element in the No-BF case, 4 elements in the 2x2 and 1x4 cases, to 16 elements in the 4x4 case.

Finally, to compare between the impact of the linear and planar array arrangement on the performance, we consider the 2x2 and the 1x4 UE array configurations where in both cases the number of antenna elements in the array is 4. It is clear from the graphs of Fig. 9 that the planar array provides slightly better performance than the linear array. This is because the linear array applies BF in one plane only (elevation or azimuth) while the planar array performs BFs in both planes.

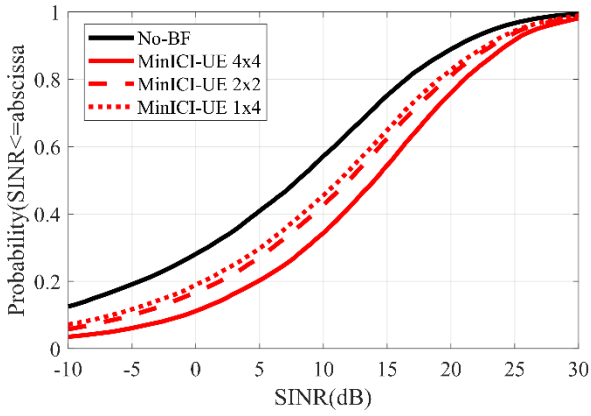

a

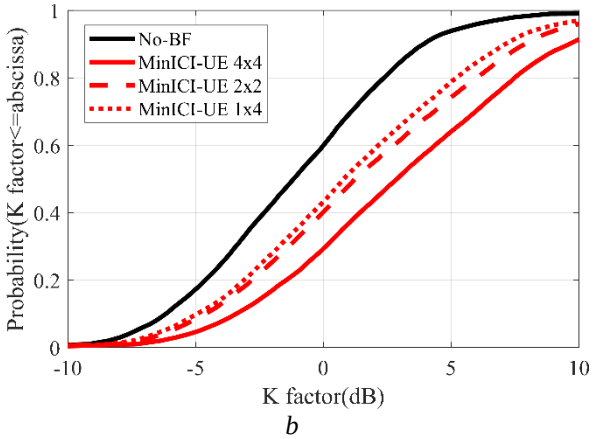

b

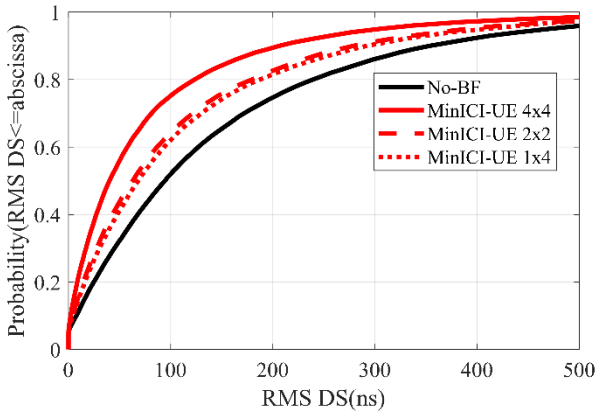

c

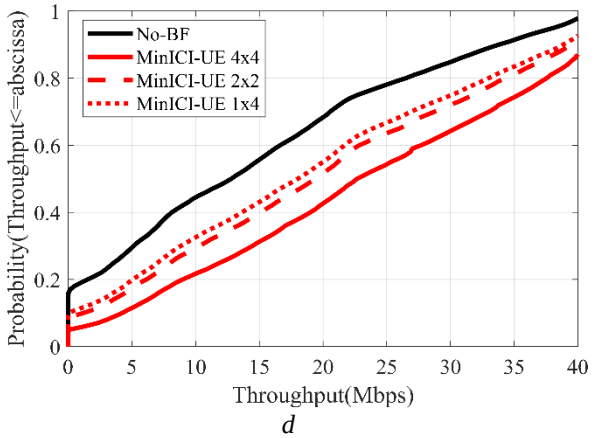

d

Fig. 9. *Performance of MinICI BF algorithm for different array configuration with a BS antenna height of 10 m.*
(a) CDF of the SINR level at the UEs.
(b) CDF of the K factor at the UEs.
(c) CDF of RMS Delay Spread (DS) at the UEs.
(d) CDF of the of UEs Throughput.

5. Conclusions

In this paper, the performance of an LTE-Advanced homogenous network deployment was evaluated assuming a frequency reuse factor of one in terms of average spectrum efficiency, cell edge throughput and outage probability using a PDSCH abstraction engine simulator. The communication channel between the main BS-UE links and the interfering BS-UE links were modelled using a site-specific map-based 3D ray-tracing tool based on realistic city-centre scenario in Bristol. The study was performed for various cell diameters, and BS antenna heights at a carrier frequency of 2.6 GHz. Linear and planar arrays were deployed at the BS and UE sides of the link with two proposed BF algorithms applied to increase system performance. Results were also compared against a previously reported three-sector FFR technique. The following conclusions can be drawn:

- When ISI and IsecI are considered, better network performance was achieved for BS heights of 10 m (compared with 30 m and 50 m). This occurred because of the higher path loss experienced by the interfering BS-UE links compared to the main BS-UE links at lower BS heights.
- Planar antenna arrays and analogue beamforming at the BS and UE represent a promising technology to meet the capacity requirements of future networks. The benefits are particularly compelling for cell edge users, where there is no requirement to increase BS transmit powers or to partition the available spectrum.
- The increase in the number of the antenna elements in the array provides improved effective K factor and RMS delay spread as well as increased throughput and SINR level at the UE.
- Unlike other ICI mitigation methods (including BS controlled BF), the MinICI-BF algorithm does not require information feedback between the UEs and the BSs. Given the advancements being made in digital signal processing and electronic circuit fabrication it is now possible to integrate 2×2 arrays into smartphone UEs and 4×4 arrays into tablet UEs.

6. Acknowledgments

Araz Sabir Ameen would like to thank the University of Sulaimani and the HCDP directorate at the Ministry of Higher Education and Scientific Research in Kurdistan of Iraq for sponsoring his PhD study.

7. References

[1] 3GPP TR36.913-V10: 'Requirements for Further Advancements for Evolved Universal Terrestrial Radio Access; (LTE Advanced-Release10) ', 2011.

[2] Himayat, N., Talwar, S., Rao, A., *et al.*: 'Interference Management for 4G Cellular Standards', IEEE Communications Magazine, 2010, 48, (8), pp. 86 - 92.

[3] 3GPP TS36.942-V10.2: 'Evolved Universal Terrestrial Radio Access: Radio Frequency System Scenarios', 2010.

[4] 3GPP TS36.300-V10.7: 'Evolved Universal Terrestrial Radio Access and Evolved Universal Terrestrial Radio Access Network: Overall Description; Stage2', 2012.

[5] 3GPP TR36.819-V11.2: 'Coordinated Multi-Point Operation for LTE Physical Layer Aspects', 2013.

[6] 3GPP TR36.829-V11.1: 'Enhanced Performance Requirement for LTE User Equipment', 2012.

[7] Sun, S., Gao, Q., Peng, Y., *et al.*: 'Interference Management Through CoMP in 3GPP LTE-Advanced Networks', IEEE Wireless Communications Magazine, 2013, 20, (1), pp. 59 - 66.

[8] 3GPP TR36.866-V12: 'Study on Network Assisted Interference Cancellation for LTE', 2014.

[9] Hardouin, E., Hassan M., Saadani A.: 'Downlink Interference Cancellation in LTE: Potential and Challenges', Proc. Int. Conf. Wireless Communications and Networking Conference(WCNC), Shanghai, China, April 2013, pp. 3597-3602.

[10] Zhou, G., Xu, W. Bauch, G.: 'Network Assisted Inter-Cell Codeword Cancellation for Interference-Limited LTE-A and Beyond', Proc. Int. Conf. Wireless Communications and Networking Conference Workshops (WCNCW), Istanbul, Turkey, April 2014, pp. 52-57.

[11] Gupta, V., Nambiar, A., Kasbekar, G.: 'Complexity Analysis, Potential Game Characterization and

Algorithms for the Inter Cell Interference Coordination with Fixed Transmit Power Problem', *IEEE Transactions on Vehicular* Technology,2017, DOI: 10.1109/TVT.2017.2774862.

[12] Lee, W., Choi, H., Kim, H., et al.: 'Adaptive Sector Coloring Game for Geometric Network Information-Based Inter-Cell Interference Coordination in Wireless Cellular Networks', IEEE/ACM Transactions on Networking, 2018, 26, (1), pp. 288-301.

[13] Qian, M., Hardjawana, W., Li, Y., *et al.*: 'Adaptive Soft Frequency Reuse Scheme for Wireless Cellular Networks', IEEE Transactions on Vehicular Technology, 2015, 64, (1), pp. 118 -131.

[14] Boudreau, G., Panicker, J., Guo, N., *et al.*: 'Interference Coordination and Cancellation for 4G Networks', IEEE Communications Magazine, 2009, 47, (4), pp. 74 - 81.

[15] Sheu, J., Lyu, S., Huang, C.: 'On antenna orientation for inter-cell interference coordination in cellular network MIMO systems', Journal of Communications and Networks, 2016, 18, (4), pp. 639-648.

[16] 3GPP TS36.211-V10.4: 'Evolved Universal Terrestrial Radio Access: Physical Channels and Modulation', 2011.

[17] Sun, S., Rappaport, T., Heath, R., *et al.*: 'MIMO for Millimeter-Wave Wireless Communications: Beamforming, Spatial Multiplexing, or Both?', IEEE Communications Magazine, 2014, 52, (12), pp.110 - 121.

[18] Sohrabi, F., Yu, W.: 'Hybrid Digital and Analog Beamforming Design for Large-Scale Antenna Arrays', IEEE Journal of Selected Topics in Signal Processing, 2016, 10, (3), pp. 501-513.

[19] Bai, T., Alkhateeb, A., Heath, R.: 'Coverage and Capacity of Millimeter-Wave Cellular Networks', IEEE Communications Magazine, 2014,52, (9), pp. 70-77.

[20] Choi, J.: 'Analog Beamforming for Low-Complexity Multiuser Detection in mm-Wave Systems', IEEE Transactions on Vehicular Technology, 2016, 65, (8), pp. 6747-6752.

[21] Hur, S., Kim, T., Love, D., *et al.*: 'Millimeter Wave Beamforming for Wireless Backhaul and Access in Small Cell Networks', IEEE Transactions on Communications, 2013, 61, (10), pp. 4391- 4403.

[22] Via, J., Santamaria, I., Elvira, V., *et al.*: 'A General Criterion for Analog Tx-Rx Beamforming Under OFDM Transmissions', IEEE Transactions on Signal Processing, 2010, 58, (4), pp. 2155-2167.

[23] Ma, X., Lu, L., Sheng, W., *et al*: 'Adaptive interference nulling with pattern maintaining under main lobe subspace and quadratic constraints', IET Microwaves, Antennas & Propagation, 2018, 12, (1), pp. 40-48.

[24] Tameh, E., Nix, A.: 'The Use of Measurement Data to Analyse the Performance of Rooftop Diffraction and Foliage Loss algorithms in a 3-D Integrated Urban/Rural Propagation Model', Proc. Int. Conf. Vehicular Technology Conference (VTC), Ottawa, Canada, May 1998, pp. 303-307.

[25] 'High-Capacity Indoor Wireless Solutions: Picocell or Femtocell?', www.fujitsu.com/us/Images/High-Capacity-Indoor-Wireless.pdf, accessed April 2015.

[26] Balanis, C.: 'Arrays: Linear, Planar, and Circular', in: 'Antenna Theory: Analysis and Design' (John Wiley & Sons, New York, 1997, 2nd edn.), pp. 249-320.

[27] Mellios, E., Mansor, Z., Hilton, G., *et al.*: 'Impact of Antenna Pattern and Handset Rotation on Macro-cell and Pico-cell Propagation in Heterogeneous LTE networks', Proc. Int. Symp. Antennas and Propagation, Chicago, USA, July 2012.

[28] Wan, L., Tsai, S., Almgren, M.: 'A Fading-Insensitive Performance Metric for a Unified Link Quality Model', Proc. Int. Conf. Wireless Communications and Networking Conference (WCNC), Las Vegas, USA, April 2006, pp. 2110-2114.

[29] Ameen, A., Mellios, E., Doufexi, A., *et al.*: 'LTE Advanced Downlink Throughput Evaluation in the 3G and TV White Space Bands', Proc. Int. Symp. Personal Indoor and Mobile Radio Communications (PIRMC), London, UK, September 2013, pp. 771-775.

[30] Beh, K., Doufexi, A., Armour, S.: 'Performance Evaluation of Hybrid ARQ Schemes of 3GPP LTE OFDMA System', Proc. Int. Symp. Personal Indoor and Mobile Radio Communications (PIMRC), Athens, Greece, September 2007, pp. 1-5.

[31] Saquib, N., Hossain, E., Kim, D.: 'Fractional Frequency Reuse for Interference Management in LTE-advanced HetNets', IEEE Wireless Communications Magazine, 2013, 20, (2), pp. 113-122.